

# Zero-Shot Autonomous Vehicle Policy Transfer: From Simulation to Real-World via Adversarial Learning

Behdad Chalaki, Logan Beaver, Ben Remer, Kathy Jang, Eugene Vinitzky,  
Alexandre Bayen, Andreas A. Malikopoulos

**Abstract**—In this paper, we demonstrate the first successful zero-shot transfer of an autonomous driving policy directly from simulator to a scaled autonomous vehicle under stochastic disturbances. Using adversarial multi-agent reinforcement learning, in which an adversary perturbed both the inputs and outputs of the autonomous vehicle during training, we train an autonomous vehicle to manage a roundabout merge in the presence of an adversary in simulation. At test time, the adversarial policy successfully reproduces the simulated ramp metering behavior and outperforms both a human driving baseline and adversary-free trained policies. Finally, we demonstrate that the addition of adversarial training considerably improves the stability and robustness of policies being transferred to the real world. Supplementary information and videos can be found at: <https://sites.google.com/view/ud-ids-lab/arlv>.

## I. INTRODUCTION

In the past century, traffic systems have become a significant concern in metropolitan areas. In 2015, commuters in urban US areas spent an estimated 6.9 billion additional hours waiting in congestion, resulting in an extra 3.1 billion gallons of fuel costing an estimated \$160 billion [1]. The dominant sources of congestion in urban networks are merging roadways, intersections, and roundabouts which act as bottlenecks on the high-capacity roadways [2].

Emergence of information and communication technologies is a promising way to mitigate congestion and enable vehicles to respond rapidly to changes in their environment. The use of connected and automated vehicles (CAVs) can aim at transitioning into an energy-efficient mobility system. Introducing CAVs into transportation system allows users to make better operational decisions, leading to large reductions of energy consumption, greenhouse gas emissions, and travel delays alongside significant improvements to passenger safety [3]. Additionally, the generation of massive amounts of vehicle data creates significant opportunities to develop optimization algorithms for controlling large-scale behaviors for entire urban systems. The Japan ITS Energy Project [4], the Safe Road Trains for the Environment

program [5], and the California Partner for Advanced Transportation Technology [6], are among the mostly-reported efforts in the area, used automated transportation to increase throughput and improve safety.

There have been two major approaches of using CAVs to improve both safety and efficiency of the total transportation system. The first approach is based on connectivity and automation being used to reduce vehicle gaps and form high-density vehicle platoons. The idea of introducing these platoons to transportation network gained momentum in the 1980s and 1990s [7], [8] as a method to alleviate congestion. The second approach is smoothing the flow of traffic to eliminate stop-and-go driving by optimal coordination through traffic bottlenecks. Stern et al. [9] demonstrated how insertion of a single AV following a classical control policy into a ring road of human-driven vehicles can diminish the stop-and-go waves.

Several efforts have been reported in the literature towards coordinating CAVs to reduce spatial and temporal speed variation of individual vehicles throughout the network. These variations can be introduced to the system through the environment, such as by breaking events, or due to the structure of the road network, e.g., intersections [10]–[12], cooperative merging [13]–[15], and speed harmonization, through optimal vehicle control [16]. One of the earliest efforts in this direction was proposed by Athans [17] to efficiently and safely coordinate merging behaviors as a step to avoid congestion. With an eye toward near-future CAV deployment, several recent studies have explored the traffic and energy implications of partial penetration of CAVs under different transportation scenarios, e.g., [18]–[20]. Recent survey papers that report the details of these efforts in this area can be found in [21]–[23]. While classical control is an continuously effective method for some traffic control tasks, the complexity and sheer problem size of autonomous driving in mixed-traffic scenarios make it a notoriously difficult problem to solve.

In recent years, deep reinforcement learning (RL) has emerged as a alternative method for traffic control. RL is recognized for its ability to solve data-rich, complex problems such as robotic skills learning [24], to larger and more difficult problems such as learning winning strategies for Go [25] or StarCraft II [26]. Deep RL is capable of handling highly complex behavior-based problems, and thus naturally extends to traffic control.

The results from the ring road experiments that Stern and Sugiyama [9], [27] demonstrated their classical control

This research was funded in part by the Delaware Energy Institute (DEI) and in part by an NSF Graduate Research Fellowship. AWS credits and funding were provided by an Amazon Machine Learning Research award.

Behdad Chalaki, Logan Beaver, Ben Remer, and Andreas A. Malikopoulos are with the Department of Mechanical Engineering, University of Delaware, Newark, DE, USA (email: bchalaki@udel.edu, lebeaver@udel.edu, bremer@udel.edu, andreas@udel.edu).

Kathy Jang, Eugene Vinitzky, and Alexandre Bayen are with the Department of Electrical Engineering and Computer Sciences, University of California, Berkeley, CA, USA (email: kathyjang@berkeley.edu, evinitzky@berkeley.edu, bayen@berkeley.edu).

policies have also been achieved via RL methods [28]. AVs, controlled with RL-trained policies, have been further used to demonstrate the traffic-smoothing capabilities of AVs in simple traffic scenarios such as figure eight road networks [28], intersections [29] and roundabouts [30], and can also replicate traffic light ramp metering behavior [31]. CAV technology surrounding traffic lights has shown to reduce fuel consumption by 50–57% while maintaining arrival time [32]. Indeed, evaluation and validation control approaches under different traffic scenarios with using hardware is an inevitable task to assure successful implementation of algorithms.

The contributions of this paper are:

- The introduction of an adversarial multi-agent policy to learn a robust emergent ramp metering behavior.
- The demonstration of small disturbances leading to poor system performance for policies with simple noise injection on a single-agent policy.
- Experimental demonstration of how an autonomous vehicle can significantly improve performance in a mixed-traffic system.

The remainder of this paper is organized as follows. In Section II, we provide background information on reinforcement learning, car following model, the FLOW framework, and the experimental testbed. In Section III, we introduce the mixed-traffic roundabout problem and the implementation of the RL framework. In Section IV, we present the simulation results and, in Section V, we discuss the policy transfer process along with the experimental results. Finally, we draw concluding remarks in Section VI.

## II. BACKGROUND

### A. Deep Reinforcement Learning

RL is a subset of machine learning which studies how an agent can take actions in an environment to maximize its expected cumulative reward. The environment in which RL trains its agent is formalized as a *Markov Decision Processes* (MDPs) [33], a framework for discrete time stochastic control processes. A finite-horizon, discounted MDP, which is the model used for all experiments in this article, is defined by the tuple  $(\mathcal{S}, \mathcal{A}, P, r, \rho_0, \gamma, T)$ . The variables in this tuple are defined as follows:  $\mathcal{S} \subseteq \mathbb{R}^n$  is an  $n$ -dimensional set of states,  $\mathcal{A} \subseteq \mathbb{R}^m$  is an  $m$ -dimensional set of actions,  $P : \mathcal{S} \times \mathcal{A} \times \mathcal{S} \rightarrow \mathbb{R}_{\geq 0}$  describes the transitional probability of moving from one state  $s$  to another state  $s'$  given action  $a$ ,  $r : \mathcal{S} \times \mathcal{A} \rightarrow \mathbb{R}$  is the reward function,  $\rho_0 : \mathcal{S} \rightarrow \mathbb{R}_{\geq 0}$  is the probability distribution over start states,  $\gamma \in (0, 1]$  is the discount factor, and  $T$  is the horizon.

In RL, an agent iteratively receives sensory information describing its environment in the form of  $\mathcal{S}$ . Based on  $\mathcal{S}$ , the agent decides on what actions  $\mathcal{A}$  to take to advance to the following state  $s'$ . These actions are chosen from a stochastic policy  $\Pi : \mathcal{S} \rightarrow \mathcal{A}$ . The goal of RL is to learn an optimal policy  $\Pi^* : \mathcal{S} \rightarrow \mathcal{A}$  by maximizing  $R = \mathbb{E} \left[ \sum_{t=0}^T \gamma^t r_t \right]$ , where  $r_t$  is the reward received at time  $t$ . This goal learns

the best actions to take from any given state to maximize the expected cumulative reward.

Deep RL is a form of RL which parameterizes the policy  $\Pi$  with the weights of a neural net. The neural net consists of an input layer, which accepts state inputs  $s \in \mathcal{S}$ ; an output layer, which returns actions  $a \in \mathcal{A}$ ; and hidden layers, consisting of affine transformations and non-linear activation functions. The flexibility that hidden layers provide neural nets with a basis for being *universal function approximators*, and enables RL policies to achieve a more expressive form.

### B. Policy Gradient Algorithms

There are a number of algorithms that exist for deriving an optimal RL policy  $\Pi^*$ . For the experiments in this article,  $\Pi^*$  is learned via either *Proximal Policy Optimization* (PPO) [34] or *Trust Region Policy Optimization* (TRPO) [35], both policy gradient algorithms. Policy gradient algorithms operate in the policy space by computing an estimate of the gradient of the expected reward  $\nabla_{\theta} R = \nabla_{\theta} \mathbb{E} \left[ \sum_{t=0}^T \gamma^t r_t \right]$ , where  $\theta$  is the parameters of the policy. The policy is then updated by performing gradient ascent methods to update  $\theta$ .

In this article, we use two forms of policy gradient for the two types of experiments described in Sec. III, Gaussian single-agent and adversarial multi-agent. TRPO is the policy gradient algorithm used for Gaussian single-agent experiments. TRPO guarantees monotonic policy improvements, and bounds updates by a *trust region*, which prevents the KL divergence between policy update from shifting too sharply. The policy gradient algorithm used for adversarial multi-agent experiments is PPO, which uses a clipped surrogate objective and multiple epochs of stochastic gradient ascent to perform each policy update, giving it a stability and reliability similar to trust region methods such as TRPO.

### C. Car Following Models

We used the *Intelligent Driver Model* (IDM) [36] as the model of the human driving dynamics. IDM is a time-continuous microscopic car-following model which is widely used in vehicle motion modeling. Using the IDM, the acceleration for vehicle  $\alpha$  is a function of its distance to the preceding vehicle, or the *headway*  $s_{\alpha}$ , the vehicle's own velocity  $v_{\alpha}$ , and *approaching rate*, or relative velocity,  $\Delta v_{\alpha}$ , namely,

$$a_{\text{IDM}} = \frac{dv_{\alpha}}{dt} = a \left[ 1 - \left( \frac{v_{\alpha}}{v_0} \right)^{\delta} - \left( \frac{s^*(v_{\alpha}, \Delta v_{\alpha})}{s_{\alpha}} \right)^2 \right], \quad (1)$$

where  $s^*$  is the desired headway of the vehicle and is given

$$s^*(v_{\alpha}, \Delta v_{\alpha}) = s_0 + \max \left( 0, v_{\alpha} T + \frac{v_{\alpha} \Delta v_{\alpha}}{2\sqrt{ab}} \right), \quad (2)$$

where  $s_0, v_0, T, \delta, a, b$  are known parameters. We describe these parameters and the values used in our simulation in Section IV.

#### D. Flow

For the training of the RL policies in this paper, we used *Flow* [37], an open-source framework for interfacing RL libraries such as RLlib [38] and rllab [39] with traffic simulators such as SUMO [40] or Aimsun. *Flow* enables the ability to design and implement RL solutions for a flexible, wide variety of traffic-oriented scenarios. RL environments built using *Flow* are compatible with OpenAI Gym [41] and as such, support training with most RL algorithms. *Flow* also supports large-scale, distributed computing solutions via AWS EC2.<sup>1</sup>

### III. PROBLEM FORMULATION

To demonstrate the viability of autonomous RL vehicles in smoothing and reducing mixed traffic, the scenario depicted in Fig. 1 was implemented. In this scenario, two groups of vehicles enter the roundabout stochastically, one at the northern end and one at the western end. In what follows, we refer to the vehicles entering from the northern end as the *northern group*, and to the vehicles entering from the western end as the *western group*.

The baseline scenario consists of homogeneous human-driven vehicles using the IDM controller (1). During the baseline it is likely that several vehicles at the northern entrance must yield to roundabout traffic, resulting in significant travel delays. The RL scenario puts an autonomous vehicle at the head of each group, which can be used to control and smooth the interaction between vehicles; these mixed experiments correspond to a 15 – 50% mixture of autonomous and human driven vehicles.

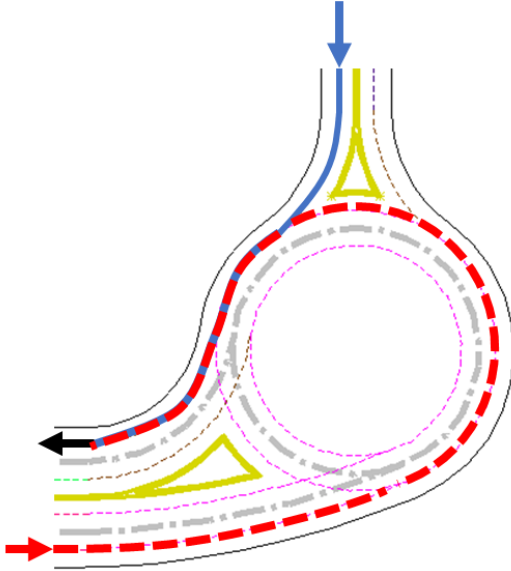


Fig. 1. The route taken by the northern and western groups through the roundabout.

<sup>1</sup>For further information on Flow, we refer readers to view the *Flow* Github page, website, or article, respectively listed here. Github: <https://github.com/flow-project/flow>, website: <https://flow-project.github.io/>, paper: [37].

#### A. Reinforcement Learning Structure

We categorize two sets of RL experiments that are used and compared in this paper, and will refer to them as:

- 1) Gaussian single-agent: A single-agent policy trained with Gaussian noise injected into the state and action space
- 2) Adversarial multi-agent: A multi-agent policy trained wherein one of 2 agents provides selective adversarial noise to the original agent

We will discuss the particulars of these two methods in Sections III-A.4 and III-A.5. In this paper, we deploy seven RL-trained policies, one of which is single-agent with no noise, three of which are Gaussian single-agent and the other three of which are adversarial multi-agent. All experiments follow the same setup. Inflows of stochastic length emerge at the northern and western ends of the roundabout. For the northern group emerging from the northern end, the range of the group will range from  $[2, 5]$ , while the range of the inflows of the western group ranges from  $[2, 8]$ . The length of these inflows will remain static across each rollout, and are randomly selected at the beginning of each new rollout.

1) *Action Space*: The actions are applied from a 1-dimensional vector of length two, in which the first element is used to control the AV leading the northern group, and the second is used to control the AV leading the western group. Due to the limitation of having a fixed-size action vector, a maximum of 2 AVs can have RL control. To oversee this, two first-in-first-out (FIFO) queues are maintained during training to keep track of AVs in the system that are capable of RL control. One queue maintains a history of vehicles entering from the northern entry, and the other maintains a history of vehicles entering from the western entry. When an AV leaves the system, it is popped from its corresponding queue. The acceleration from the action vector is applied to the first vehicle in either queue, and is simply discarded if the queue is empty. While in the final policies we present in this article, there is never more than 1 vehicle per queue, this design is necessary to support the early stages of training when traffic jams occur frequently, and each queue is populated at 2+.

2) *State Space*: The state space conveys the following information about the environment to the agent:

- The positions of the AVs.
- The velocities of the AVs.
- The distances from the roundabout of the 6 closest vehicles to the roundabout for both roundabout entryways.
- The velocities of the 6 closest vehicles to the roundabout for both roundabout entryways.
- Tailway and headway (i.e. distances to the leading and following vehicles) of vehicles from both AVs.
- Length of the number of vehicles waiting to enter the roundabout for both roundabout entryways.
- The distances and velocities of all vehicles in the roundabout.
- Lengths of the incoming inflows

All elements of the state space are normalized. The state space was designed with real-world implementation in mind.

As such, it is partially-observable to support modern sensing capabilities. All of these observations are reasonably selected, and could be emulated in the physical world using sensing tools such as induction loops, camera sensing systems, and speedometers.

3) *Reward Function*: The reward function used for all experiments minimizes delay and applies penalties for standstill velocities, near-standstill velocities, jerky driving, and speeding.

$$r_t = 2 \cdot \frac{\max \left( v_{\max} \sqrt{n} - \sqrt{\sum_{i=1}^n (v_{i,t} - v_{\max})^2}, 0 \right)}{v_{\max} \sqrt{n}} - p. \quad (3)$$

In this reward function,  $p$  is defined to be the sum of 4 different penalty functions, or  $p = p_s + p_p + p_j + p_v$ , where  $p_s$  is a penalty for vehicles traveling at zero velocity, designed to discourage standstill;  $p_p$  penalizes vehicles traveling below  $0.2m/s$ , which discourages the algorithm from learning a RL policy which substitutes extremely low velocities to circumvent the zero-velocity penalty;  $p_j$  discourages jerky driving by maintaining a dynamic queue containing the last 10 actions and penalizing the variance of these actions; and  $p_v$  penalizes speeding.

4) *Gaussian single-agent noise*: Injecting noise directly to the state and action space has been shown to aid with transfer from simulation to real world testbeds [30], [42]. In this method, which applies to 3 of the policies we deployed, each element of the state space was perturbed by a random number selected from a Gaussian distribution with a standard deviation= 0.1. Each element of the action space was perturbed by a random number selected from a Gaussian distribution with standard deviation= 0.5.

5) *Adversarial multi-agent noise*: For the other 3 policies, we use a form of adversarial training to yield a policy resistant to noise [43]. This is a form of multi-agent RL, in which two policies are learned. Adversarial training pits two agents against each other in a zero-sum game. The first is structurally the same as the agent which is trained in the previous 4 policies. The second, *adversarial* agent has a reward function that is the negative of the first agent's reward; in other words, it is incentivized by the first agent's failure. The adversarial agent can do this by perturbing elements of the action and state space of the first agent.

The adversarial agent's action space is a 1-dimensional vector of length 22, composed of perturbation values bound by  $[-1, 1]$ . The first 2 elements of the adversarial action space are used to perturb the action space of the original agent's action space, which is of length 2. Adversarial action perturbations are scaled down by 0.1. Combining adversarial training with selective randomization, the adversarial agent has access to perturb a subset of the original agent's state space. The remaining 20 elements of the adversarial agent space are used to perturb 20 selective elements of the original agent's state space. Adversarial state perturbations are scaled down by 0.2. These selective elements are described below:

- The positions and velocities of both controlled AVs in the system.

- The distances of vehicles from the merge points.

## IV. SIMULATION FRAMEWORK

### A. Car Following Parameters

As introduced in Section II-C, the human-driven vehicles in these simulations are controlled via IDM. Accelerations are provided to the vehicles via equations 1 and 2. Within these equations,  $s_0$  is the minimum spacing, or minimum desired net distance from the vehicle in front of it,  $v_0$  is the desired velocity,  $T$  is the desired time headway,  $\delta$  is an acceleration exponent,  $a$  is the maximum vehicle acceleration, and  $b$  is the comfortable braking deceleration.

Human-driven vehicles in the system operate using SUMO's built-in IDM controllers, which allows customization to the parameters described above. Standard values for these parameters as well as detailed discussion on the experiments producing these values can be found in [36]. In these experiments, the parameters of the IDM controllers are defined to be  $T = 1$ ,  $a = 1$ ,  $b = 1.5$ ,  $\delta = 4$ ,  $s_0 = 2$ ,  $v_0 = 30$ .

To model the natural variance in human driving behavior, we supply stochasticity to SUMO's IDM controller by setting  $noise = 0.1$ . In doing this, for every human-vehicle acceleration, SUMO samples from a zero-mean Gaussian distribution with a variance indicated by the value of  $noise$ , and perturbs the acceleration by this amount.

Environment parameters in simulation were set to match the physical constraints of the experimental testbed. These include: a maximum acceleration of  $1 \frac{m}{s^2}$ , a maximum deceleration of  $-1 \frac{m}{s^2}$ , and a maximum velocity of  $8 \frac{m}{s}$ . The timestep of the system is set to 1.0 seconds.

### B. Algorithm/Simulation Details

We ran both PPO and TRPO experiments with a discount factor of 0.999, a trust-region size of 0.01, a batch size of 20000, a horizon of 500 seconds, and trained over 100 iterations. The controller is a neural network, a *Gaussian multi-layer perceptron* (MLP) with a tanh non-linearity, and hidden sizes of (100, 50, 25). The choice of neural network non-linearities, size, and type were picked based on traffic controllers developed in [29]. The states are normalized so that they are between 0 and 1 by dividing each states by its maximum possible value. The actions are clipped to be between  $-1$  and  $1$ . Both normalization and clipping occur after the noise is added to the system so that the bounds are properly respected.

### C. Code Reproducibility

The following codebases are needed to reproduce the results of our work. *Flow*<sup>2</sup>, *SUMO*<sup>3</sup> and the versions of *rllab*<sup>4</sup> and *RLlib*<sup>5</sup> used for the RL algorithms is available on GitHub.

<sup>2</sup><https://github.com/flow-project/flow>.

<sup>3</sup><https://github.com/eclipse/sumo> at commit number 1d4338ab80.

<sup>4</sup><https://github.com/cathywu/rllab-multiagent> at commit number 4b5758f.

<sup>5</sup>[https://github.com/flow-project/ray/tree/ray\\_master](https://github.com/flow-project/ray/tree/ray_master) at commit number ce606a9.



#### D. Simulation Results

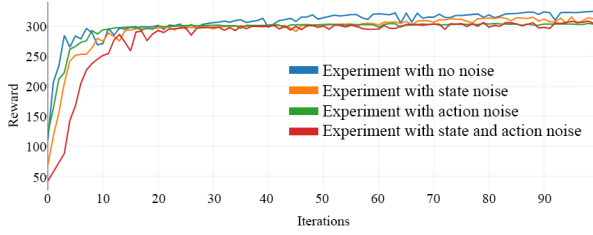


Fig. 2. Convergence of the RL reward curves of the 3 Gaussian single-agent experiments and the single-agent policy trained sans noise. The curves are superimposed.

The reward curves of the Gaussian single-agent experiments are displayed in Fig. 2. These include the curves of the 3 experiments which are trained with Gaussian noise injection, as well as one trained without any noise. While the curves of the 3 noised experiments converge to a similar value, the beginning stages of training can portray how noise causes the initial stages to either perform noticeably worse or take longer to train.

In both the Gaussian single-agent and adversarial multi-agent experiments, the policy learns a classic form of traffic control: ramp-metering, in which one group of vehicles slows down to allow for another group of vehicles to pass. Despite the varying length of inflows from the north and western entries, policies consistently converge to demonstrate ramp-metering.

#### V. EXPERIMENTAL DEPLOYMENT

##### A. The University of Delaware's Scaled Smart City

The University of Delaware Scaled Smart City (UDSSC) (Fig. 4) is a 1 : 25 scale testbed designed to replicate real-world traffic scenarios and implement cutting-edge control technologies in a safe and scaled environment. UDSSC is a fully integrated smart city, which can be used to validate the efficiency of control and learning algorithms, and their applicability in hardware. UDSSC utilizes high-end computers, a VICON motion capture system, and scaled CAVs to simulate a variety of control strategies with as many as 35 scaled CAVs.

The scaled CAVs have been designed using easily assembled off-the-shelf components coupled with several 3D printed parts (Fig. 5). Each CAV consists of two primary boards, a 75.81 : 1 geared differential driven Pololu Zumo and a Raspberry Pi 3B with a 1.2 GHz quad-core ARM processor and a 2.4GHz WiFi adapter used to communicate with the central *mainframe* computer (Processor: Intel Core i7-6950X CPU @ 3.00 GHz x 20, Memory: 125.8 Gb). A power regulator manages the voltage input of the Raspberry Pi and Zumo, supplying a regulated 5VDC from a 7.4VDC, 1000mAh Li-Po battery. With this hardware configuration, each CAV is able to run and collect data for approximately 90 minutes. The Pololu Zumo is equipped with a built-in dual H-bridge motor driver, on-board encoder, internal IMU,

ultrasonic sensor and an Atmega 32U4 micro-controller. Initially, each Zumo is equipped with a track, which was replaced with rubberized wheels of radius  $r = 1.6 \text{ cm}$  mounted on the front end of the Zumo. Longitudinal stability is maintained with the use of a caster ball on the rear half of the vehicle. Each CAV, without the outer shell, has a 10.5 x 4.5 cm footprint, with a low height profile of 4.5 cm.

UDSSC utilizes a multi-level control architecture to precisely position each vehicle using position feedback from a VICON motion capture system. High level routing and steering control is handled by the mainframe computer and sent as linear and angular velocity commands to each CAV. Communication between the mainframe and each CAVs is achieved by a local WiFi network through the non-blocking, asynchronous electron package for Node.js. The vehicle information, ROS architecture, and a friendly user-interface are all combined on an HTML/CSS webpage. In the high-level control, lane and reference tracking is used to keep the vehicle in the center of its lane at a prescribed speed. This is achieved through a potential field approach, which uses the fact that roads in UDSSC are made up of arcs and line segments. Each vehicle in UDSSC has a position vector  $\mathbf{X}(t) \in \mathbb{R}^2$ , which is steered through the potential field. The direction of the field for a straight segment is

$$\mathbf{D}(t) = \hat{\mathbf{T}} + p_L \left( \mathbf{X}_0 - \mathbf{X}(t) + \mathbf{A}(t)\hat{\mathbf{T}} \right), \quad (4)$$

where  $\hat{\mathbf{T}}$  is a unit vector tangent to the line segment,  $p_L$  is a tunable convergence parameter,  $\mathbf{X}_0$  is the start of the line segment, and  $\mathbf{A}(t)$  is the 2x2 matrix given by

$$\mathbf{A}(t) = \begin{bmatrix} a(t) & 0 \\ 0 & a(t) \end{bmatrix}, \quad (5)$$

$$a(t) = [\mathbf{X}(t) - \mathbf{X}_0] \cdot \mathbf{T}. \quad (6)$$

Similarly, arc potential fields has the direction

$$\mathbf{D}(t) = \begin{bmatrix} -p_A \cdot C(t) & r \cdot cw \\ r \cdot cw & -p_A \cdot C(t) \end{bmatrix} [\mathbf{X}(t) - \mathbf{X}_c], \quad (7)$$

where  $p_A$  is a tunable convergence parameter,  $cw$  is an indicator for the arc, such that

$$cw = \begin{cases} 1 & \text{if clockwise} \\ -1 & \text{if counterclockwise} \end{cases}, \quad (8)$$

and  $C(t)$  is

$$C(t) = \left\| \mathbf{X}(t) - \mathbf{X}_c \right\| - r^2, \quad (9)$$

where  $\|\cdot\|$  is the Euclidean norm,  $\mathbf{X}_c$  and  $r$  are the center and radius of the arc respectively. An in-depth overview of this method and its application to the CAVs is described in [44], [45].

The velocity control for each non-RL vehicle is specified by the Intelligent Driver Model (1). The resulting state update is given by

$$\dot{\mathbf{X}} = v^{\text{idm}} \frac{\mathbf{D}}{\|\mathbf{D}\|}, \quad (10)$$

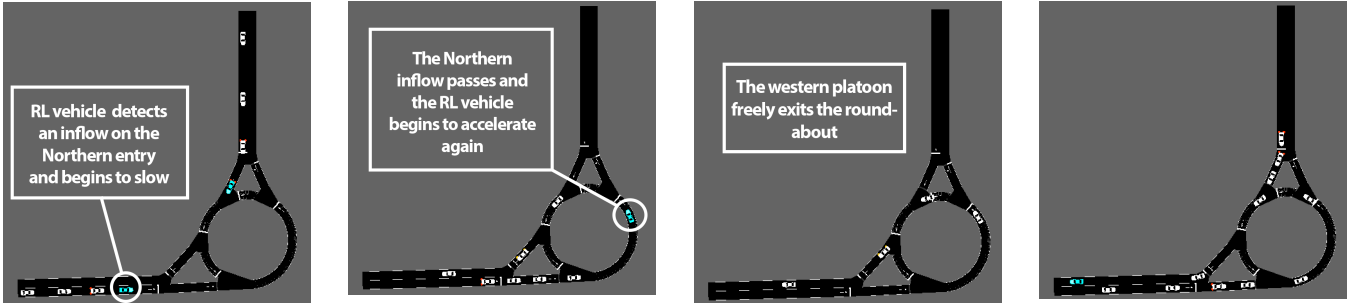


Fig. 3. Two RL-controlled AVs trained with adversarial multi-agent noise demonstrate ramp metering behavior in this series of images, followed by an image of the baseline where vehicles clash. **First:** RL vehicle slows down in anticipation of a sufficiently short inflow from the north. **Second:** The northern inflow passes through the roundabout at high velocity. **Third:** The western group exits the roundabout at high velocity. **Fourth:** The baseline in which all vehicles are human-driven results in queues and clashing groups.



Fig. 4. The University of Delaware Scaled Smart City (UDSSC).

where  $v^{idm}$  is calculated via numerical integration, and  $\mathbf{D}$  is dependent on the vehicle's location within UDSSC. This velocity is periodically sent to each CAV as a desired heading and speed command.

### B. Policy Transfer

To implement the RL policy in UDSSC, the weights of the network generated by *Flow* were exported into a '.pkl' file. This file was accessed through a python script on the mainframe which maps VICON data into the required format for the neural network input vector. This included the 2D position of each vehicle within the city, the number of vehicles at each roundabout entrance, and the current speed of each vehicle, which was calculated with finite difference.

This python script allowed the state information of the CAVs to be directly mapped to an acceleration command for the RL vehicles. This python function behaves as a control module within UDSSC, replacing the IDM controller for the lead vehicle of each group for the duration of the experiment. The size and initial position of each vehicle group was randomly selected from a uniform distribution to explore the full space in which the RL vehicle was trained.

To capture a significant number of baseline cases during

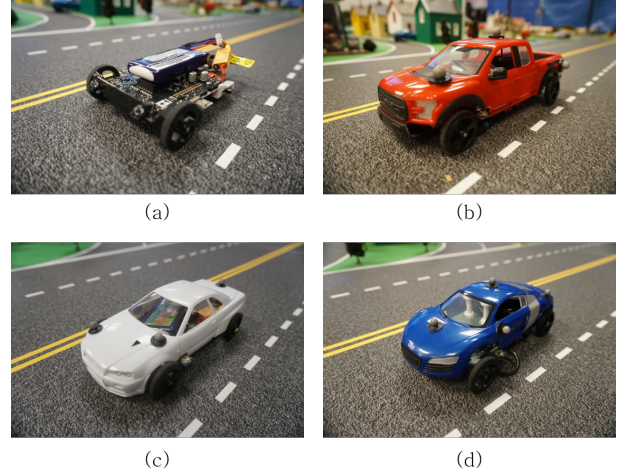


Fig. 5. A picture of the connected and automated vehicle's hardware (a) and outer shell with VICON markers (b,c,d).

the trials, a system to automatically reset the experiments was developed. After an RL experiment has completed, any vehicles which had not been selected were "flushed" through the experiment using the human-driven model. Not only did this reset the experiment, but it allowed baseline data to be collected when the number of flushed cars was sufficient (2+ north, 3+ west). In addition, a set pure baseline experiments were performed to collect data for large human-driven groups.

To generate a disturbance on the roundabout system, the initial distance of the western group was varied by a uniformly distributed  $\pm 0.5$  m during UDSSC experiments. This resulted in a uniformly distributed disturbance on the relative entrance time between the groups of  $\pm 1.67$  s.

### C. Experimental Results

The data for each vehicle was collected through the VICON motion capture system and is presented in Table I. The position of each car was tracked for the duration of each experiment, and the velocity of each car was numerically derived with a first order method. Any speed above 0.8 m/s, well above the maximum speed of each vehicle, was

considered an artifact of temporary camera occlusion and was removed. The raw position and derived velocity data were then processed through a moving average filter with a window size of 10ms to smooth out noise inherent to the system.

TABLE I

EXPERIMENTAL RESULTS FOR THE BASELINE (TOP), ADVERSARIAL NOISE (MIDDLE) AND GAUSSIAN NOISE (BOTTOM) CASES. THE ARROWS IN EACH COLUMN INDICATE CHANGE RELATIVE TO THE BASELINE.

Noise Type	Mean Time (s)	Mean Speed (m/s)	No. Trials
Baseline	25.7 —	0.29 —	71
Action-State	25.0 ↓	0.25 ↓	33
Action	29.3 ↑	0.30 ↑	16
State	28.8 ↑	0.31 ↑	8
Action-State	30.3 ↑	0.21 ↓	7
State	31.9 ↑	0.30 ↓	7
Action	39.3 ↑	0.27 ↓	8
Noiseless	34.7 ↑	0.29 —	10

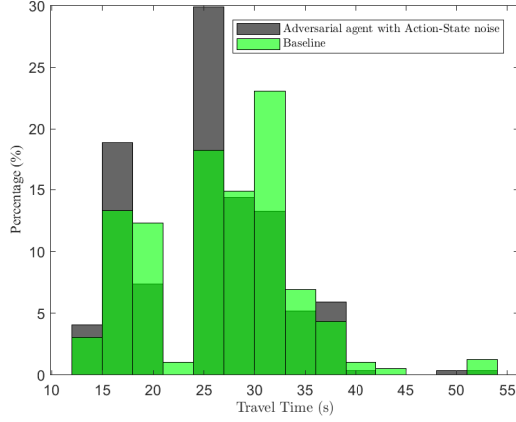


Fig. 6. Histogram for the travel time for the baseline and adversarial agent scenarios with noise injected in action and State.

For all trials, the RL vehicle exhibited the learned ramp metering behavior, where the western leader reduced its speed to avoid yielding by the northern group. The metering behavior was extreme for the Gaussian noise case, and this significantly reduced the average speed and increased travel delay, as seen in Table I. The multi-agent adversarial training significantly outperformed single agent, and tended to leave only a single vehicle yielding at the northern entrance. This strategy led to a significant travel time reduction for the northern group without a large delay on western vehicles.<sup>6</sup>

## VI. CONCLUSION

In this paper we have performed a zero shot transfer of an autonomous driving policy directly from simulator to UDSSC experimental test bed. Even under stochastic disturbances, adversarial multi-agent policy improved system efficiency by reducing travel time and average velocity for

<sup>6</sup> Videos of the experiment and supplemental information can be found at: <https://sites.google.com/view/ud-ids-lab/arlv>.

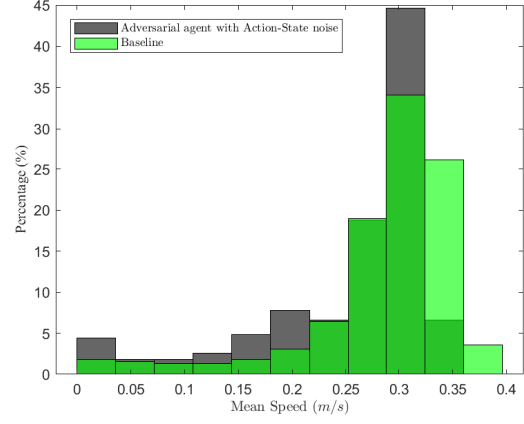


Fig. 7. Histogram of the mean speed for the baseline and adversarial agent scenarios with noise injected in action and state.

all vehicles. Finally, we demonstrated that the addition of adversarial training considerably improves the stability and robustness of policies being transferred to the real world.

As we continue to research methods of policy transfer, we aim to achieve algorithm generalization while minimizing loss of information. Some directions we hope to explore include:

- Multi-agent adversarial noise with multiple adversaries.
- Tuning to determine which elements of the state space are most suitable for perturbations.
- Tuning injected noise to maximize policy robustness.
- Larger, more complex interactions, such as intersections or highway merges.
- Longer tests involving corridors with multiple bottlenecks.

Another potential direction for future research could be the generalization of this framework to other traffic bottlenecks i.e., intersections, speed reduction zones with more complex systems including different lanes with the lane-changing ability. Furthermore, considering different penetrations of RL vehicles, which can significantly improve the efficiency of the entire network has to be studied.

## ACKNOWLEDGMENT

The authors would also like to thank Ray Zayas and Ishtiaque Mahub for their contributions to UDSSC code base.

## REFERENCES

- [1] B. Schrank, B. Eisele, T. Lomax, and J. Bak, “2015 Urban Mobility Scorecard,” tech. rep., Texas A& M Transportation Institute, 2015.
- [2] R. Margiotta and D. Snyder, “An agency guide on how to establish localized congestion mitigation programs,” tech. rep., U.S. Department of Transportation. Federal Highway Administration, 2011.
- [3] Z. Wadud, D. MacKenzie, and P. Leiby, “Help or hindrance? the travel, energy and carbon impacts of highly automated vehicles,” *Transportation Research Part A: Policy and Practice*, vol. 86, pp. 1–18, 2016.
- [4] S. Tsugawa, “An overview on an automated truck platoon within the energy its project,” *IFAC Proceedings Volumes*, vol. 46, no. 21, pp. 41–46, 2013.

- [5] A. Dávila and M. Nombela, "Sartre: Safe road trains for the environment," in *Conference on Personal Rapid Transit PRT@ LHR*, vol. 3, pp. 2–3, 2010.
- [6] S. E. Shladover, "Path at 20 history and major milestones," *IEEE Transactions on intelligent transportation systems*, vol. 8, no. 4, pp. 584–592, 2007.
- [7] S. E. Shladover, C. A. Desoer, J. K. Hedrick, M. Tomizuka, J. Walrand, W.-B. Zhang, D. H. McMahon, H. Peng, S. Sheikholeslam, and N. McKeown, "Automated vehicle control developments in the PATH program," *IEEE Transactions on Vehicular Technology*, vol. 40, no. 1, pp. 114–130, 1991.
- [8] R. Rajamani, H.-S. Tan, B. K. Law, and W.-B. Zhang, "Demonstration of integrated longitudinal and lateral control for the operation of automated vehicles in platoons," *IEEE Transactions on Control Systems Technology*, vol. 8, no. 4, pp. 695–708, 2000.
- [9] R. E. Stern, S. Cui, M. L. D. Monache, R. Bhadani, M. Bunting, M. Churchill, N. Hamilton, H. Pohlmann, F. Wu, B. Piccoli, et al., "Dissipation of stop-and-go waves via control of autonomous vehicles: Field experiments," *arXiv preprint arXiv:1705.01693*, 2017.
- [10] J. Lee and B. Park, "Development and Evaluation of a Cooperative Vehicle Intersection Control Algorithm Under the Connected Vehicles Environment," *IEEE Transactions on Intelligent Transportation Systems*, vol. 13, no. 1, pp. 81–90, 2012.
- [11] H. Rakha and R. K. Kamalanathsharma, "Eco-driving at signalized intersections using v2i communication," in *Intelligent Transportation Systems (ITSC), 2011 14th International IEEE Conference on*, pp. 341–346, IEEE, 2011.
- [12] A. A. Malikopoulos, C. G. Cassandras, and Y. Zhang, "A decentralized energy-optimal control framework for connected automated vehicles at signal-free intersections," *arXiv:1602.03786 - (provisionally accepted)*, 2017.
- [13] J. Rios-Torres and A. A. Malikopoulos, "Automated and Cooperative Vehicle Merging at Highway On-Ramps," *IEEE Transactions on Intelligent Transportation Systems*, vol. 18, no. 4, pp. 780–789, 2017.
- [14] I. A. Ntousakis, I. K. Nikolos, and M. Papageorgiou, "Optimal vehicle trajectory planning in the context of cooperative merging on highways," *Transportation Research Part C: Emerging Technologies*, vol. 71, pp. 464–488, 2016.
- [15] L. Zhao and A. A. Malikopoulos, "Decentralized optimal control of connected and automated vehicles in a corridor," in *2018 21st International Conference on Intelligent Transportation Systems (ITSC)*, pp. 1252–1257, IEEE, 2018.
- [16] A. A. Malikopoulos, S. Hong, B. Park, J. Lee, and S. Ryu, "Optimal control for speed harmonization of automated vehicles," *IEEE Transactions on Intelligent Transportation Systems*, 2018.
- [17] M. Athans, "A unified approach to the vehicle-merging problem," *Transportation Research*, vol. 3, no. 1, pp. 123–133, 1969.
- [18] L. Zhao, A. A. Malikopoulos, and J. Rios-Torres, "Optimal control of connected and automated vehicles at roundabouts: An investigation in a mixed-traffic environment," in *15th IFAC Symposium on Control in Transportation Systems*, pp. 73–78, 2018.
- [19] J. Rios-Torres and A. A. Malikopoulos, "Impact of partial penetrations of connected and automated vehicles on fuel consumption and traffic flow," *IEEE Transactions on Intelligent Vehicles*, vol. 3, no. 4, pp. 453–462, 2018.
- [20] Z. Zhong, L. Joyoung, and L. Zhao, "Evaluations of Managed Lane Strategies for Arterial Deployment of Cooperative Adaptive Cruise Control," in *TRB Annual Meeting*, (Washington DC, USA), 2017.
- [21] J. Rios-Torres and A. A. Malikopoulos, "A Survey on Coordination of Connected and Automated Vehicles at Intersections and Merging at Highway On-Ramps," *IEEE Transactions on Intelligent Transportation Systems*, vol. 18, no. 5, pp. 1066–1077, 2017.
- [22] J. Guanetti, Y. Kim, and F. Borrelli, "Control of connected and automated vehicles: State of the art and future challenges," *Annual Reviews in Control*, 2018.
- [23] Y. Wang, X. Li, and H. Yao, "Review of trajectory optimisation for connected automated vehicles," *IET Intelligent Transport Systems*, 2018.
- [24] S. Gu, E. Holly, T. Lillicrap, and S. Levine, "Deep reinforcement learning for robotic manipulation with asynchronous off-policy updates," in *Robotics and Automation (ICRA), 2017 IEEE International Conference on*, pp. 3389–3396, IEEE, 2017.
- [25] D. Silver, J. Schrittwieser, K. Simonyan, I. Antonoglou, A. Huang, A. Guez, T. Hubert, L. Baker, M. Lai, A. Bolton, et al., "Mastering the game of go without human knowledge," *Nature*, vol. 550, no. 7676, p. 354, 2017.
- [26] "Alphastar: Mastering the real-time strategy game starcraft ii," Jan 2019.
- [27] Y. Sugiyama, M. Fukui, M. Kikuchi, K. Hasebe, A. Nakayama, K. Nishinari, S.-i. Tadaki, and S. Yukawa, "Traffic jams without bottleneck experimental evidence for the physical mechanism of the formation of a jam," *New journal of physics*, vol. 10, no. 3, p. 033001, 2008.
- [28] C. Wu, A. Kreidieh, E. Vinitzky, and A. M. Bayen, "Emergent behaviors in mixed-autonomy traffic," in *Conference on Robot Learning*, pp. 398–407, 2017.
- [29] E. Vinitzky, A. Kreidieh, L. Le Flem, N. Kheterpal, K. Jang, F. Wu, R. Liaw, E. Liang, and A. M. Bayen, "Benchmarks for reinforcement learning in mixed-autonomy traffic," in *Conference on Robot Learning*, pp. 399–409, IEEE, 2018.
- [30] K. Jang, E. Vinitzky, B. Chalaki, B. Remer, L. Beaver, A. Malikopoulos, and A. Bayen, "Simulation to scaled city: zero-shot policy transfer for traffic control via autonomous vehicles," in *2019 International Conference on Cyber-Physical Systems*, (Montreal, CA), 2018.
- [31] F. Belletti, D. Haziza, G. Gomes, and A. M. Bayen, "Expert level control of ramp metering based on multi-task deep reinforcement learning," *IEEE Transactions on Intelligent Transportation Systems*, 2017.
- [32] C. Sun, X. Shen, and S. Moura, "Robust optimal eco-driving control with uncertain traffic signal timing," in *2018 Annual American Control Conference (ACC)*, pp. 5548–5553, IEEE, 2018.
- [33] R. Bellman, "A markovian decision process," *Journal of Mathematics and Mechanics*, pp. 679–684, 1957.
- [34] J. Schulman, F. Wolski, P. Dhariwal, A. Radford, and O. Klimov, "Proximal policy optimization algorithms," *arXiv preprint arXiv:1707.06347*, 2017.
- [35] J. Schulman, S. Levine, P. Abbeel, M. Jordan, and P. Moritz, "Trust region policy optimization," in *International Conference on Machine Learning*, pp. 1889–1897, 2015.
- [36] M. Treiber, A. Hennecke, and D. Helbing, "Congested traffic states in empirical observations and microscopic simulations," *Physical review E*, vol. 62, no. 2, p. 1805, 2000.
- [37] C. Wu, A. Kreidieh, K. Parvate, E. Vinitzky, and A. M. Bayen, "Flow: Architecture and benchmarking for reinforcement learning in traffic control," *arXiv preprint arXiv:1710.05465*, 2017.
- [38] E. Liang, R. Liaw, R. Nishihara, P. Moritz, R. Fox, J. Gonzalez, K. Goldberg, and I. Stoica, "Ray rllib: A composable and scalable reinforcement learning library," *arXiv preprint arXiv:1712.09381*, 2017.
- [39] Y. Duan, X. Chen, R. Houthoofd, J. Schulman, and P. Abbeel, "Benchmarking deep reinforcement learning for continuous control," in *International Conference on Machine Learning*, pp. 1329–1338, 2016.
- [40] D. Krajzewicz, J. Erdmann, M. Behrisch, and L. Bieker, "Recent development and applications of SUMO - Simulation of Urban MObility," *International Journal On Advances in Systems and Measurements*, vol. 5, pp. 128–138, December 2012.
- [41] G. Brockman, V. Cheung, L. Pettersson, J. Schneider, J. Schulman, J. Tang, and W. Zaremba, "Openai gym," *arXiv preprint arXiv:1606.01540*, 2016.
- [42] J. Tobin, R. Fong, A. Ray, J. Schneider, W. Zaremba, and P. Abbeel, "Domain randomization for transferring deep neural networks from simulation to the real world," in *Intelligent Robots and Systems (IROS), 2017 IEEE/RSJ International Conference on*, pp. 23–30, IEEE, 2017.
- [43] L. Pinto, J. Davidson, R. Sukthankar, and A. Gupta, "Robust adversarial reinforcement learning," *arXiv preprint arXiv:1703.02702*, 2017.
- [44] D. L. A. Giuseppe, Oriolo and M. Vendittelli, "Wmr control via dynamic feedback linearization: Design, implementation, and experimental validation," *IEEE Transactions on Control Systems Technology*, vol. 10, no. 6, pp. 835–852, 2002.
- [45] A. Stager, L. Bhan, A. Malikopoulos, and L. Zhao, "A Scaled Smart City for Experimental Validation of Connected and Automated Vehicles," *IFAC-PapersOnLine*, vol. 51, no. 9, pp. 130–135, 2018.